PHYSICAL REVIEW B VOLUME 31, NUMBER 7 1 APRIL 1985

Thermal conductivity of a strongly coupled plasma

George A. Rinker
Theoretical Division, Los Alamos National Laboratory, Los Alamos, New Mexico 87545

(Received 7 August 1984; revised manuscript received 5 November 1984)

This is the second in a series of papers concerning the transport properties of dense plasmas. In this work, we use the formalism of Lampe to extend our previous calculations of electrical conductivity to the calculation of thermal conductivity and thermoelectric coefficient. Quantitative results are given for iron at temperatures ranging from 10^{-2} to 10^4 eV and for densities from 3×10^{-4} to 10^5 g/cm^3.

Lampe[1] has calculated electrical and thermal transport coefficients for a weakly-coupled plasma with any degree of electron degeneracy. His calculation is carried out by solving the Lenard-Balescu equation[2] by the Chapman-Enskog method, using Fermi-statistical generalizations of the first two Sonine polynomials.

The physical models he incorporates for the electron-ion and electron-electron interactions are ultimately expressed by Coulomb logarithms. These are calculated using Born approximation with Debye-shielded potentials. The requirement of weak coupling arises principally from his use of Born approximation for the electron-ion scattering cross section, as well as the binary-collision (ring-diagram) approximation used to derive the Lenard-Balescu equation, and neglect of lattice structure at high density.

In the preceding paper[3] (referred to as I), we described a method for the complete partial-wave analysis of the Ziman formula for the electrical resistivity, using self-consistent ionic potentials, realistic structure factors, and arbitrary electron degeneracy. Further details of these calculations are given elsewhere.[4–6] Our calculations avoid the shortcomings of Born approximation and are valid for much stronger electron-ion couplings. We use an approximate scheme to compensate for some of the unphysical predictions of the average-atom model. The validity of this scheme is unknown, but we have obtained good agreement for liquid metals near the melting point. In fact, our calculations generally do as well as theoretical pseudopotential models and are surpassed only by those pseudopotential calculations that are highly parametrized to reproduce known conduction-band data.

Boercker *et al.*[7] have shown that with appropriate choices for the structure factor, the Ziman formula and the Lenard-Balescu equation are equivalent in the weak-coupling limit. This is related to the common physical approximation of sequential binary collisions. In the present work, we exploit this equivalence by combining our electrical conductivity calculations with the formal results of Lampe to obtain improved thermal transport coefficients. In our approach, we simply replace Lampe's expression for the electron-ion Coulomb logarithm with a numerical value that is adjusted to reproduce our calculated electrical conductivity. We do not modify his expression for the electron-electron Coulomb logarithm, as we expect Born approximation to be valid in that case for virtually all conditions. Thus, we obtain an internally consistent set of calculations for the ionization state, electrical conductivity, thermal conductivity, and thermoelectric coefficient. We expect these calculations to have a wider range of validity in temperature and density than previous calculations because of their fundamental basis in the partial-wave analysis of realistic electron-ion potentials. High-density effects (three-body collisions, lattice structure) related to further correlations of the electron or ion wave functions are not considered.

Lampe's coefficients are defined with respect to the transport equations

$$\mathbf{J}=eS_{11}\left[e\mathbf{E}+\frac{\nabla P}{n_e}\right]+eS_{12}\frac{\nabla T}{T}\,,$$
$$\mathbf{Q}=-S_{21}\left[e\mathbf{E}+\frac{\nabla P}{n_e}\right]-S_{22}\frac{\nabla T}{T}-\frac{5}{3}\left[\frac{\mathbf{J}}{e}\right]\epsilon\,, \tag{1}$$

where

$\mathbf{J}=$electric current ,

$-e=$electron charge ,

$\mathbf{E}=$applied electric field ,

$P=\frac{2}{3}n_e\epsilon+kT\frac{n_e}{Z}=$pressure , (2)

$n_e=$electron number density ,

$T=$temperature ,

$\mathbf{Q}=$heat flux ,

$\epsilon=$mean kinetic energy per electron .

The electrical conductivity σ and thermal conductivity κ (with the conventional constraint $\mathbf{J}=0$) are

$$\sigma=e^2S_{11}\,,$$
$$\kappa=(S_{11}S_{22}-S_{12}^2)/(TS_{11})\,. \tag{3}$$

The quantity $S_{12}=S_{21}$ will be called the thermoelectric coefficient.

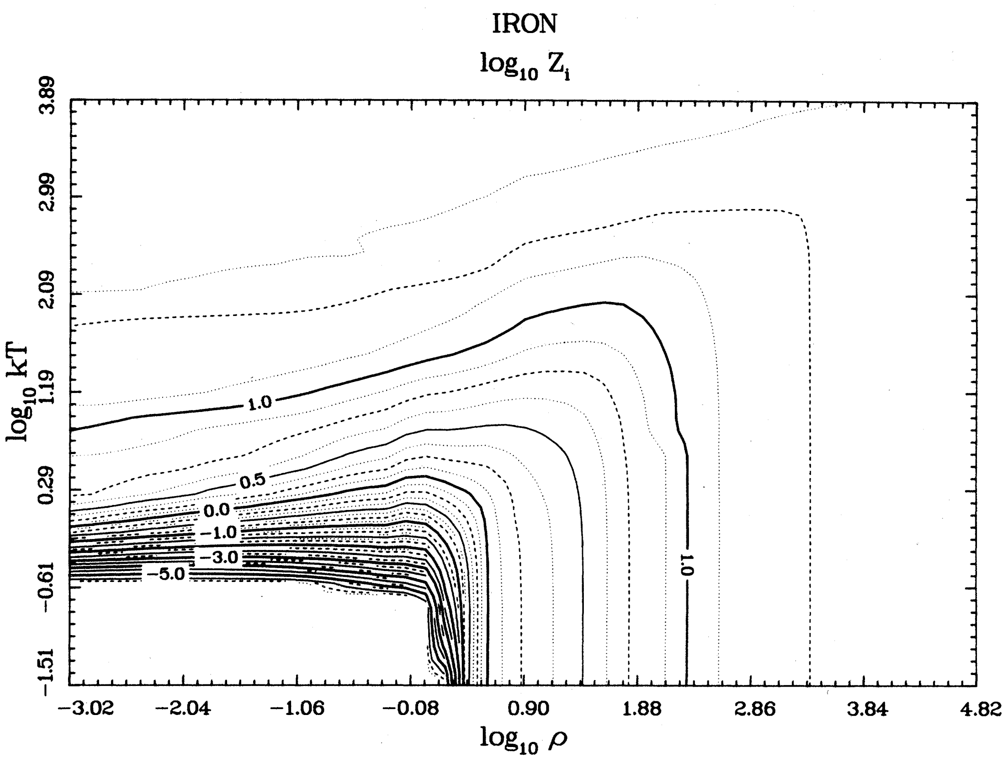

FIG. 1. Ionization state Z_i as a function of temperature and density.

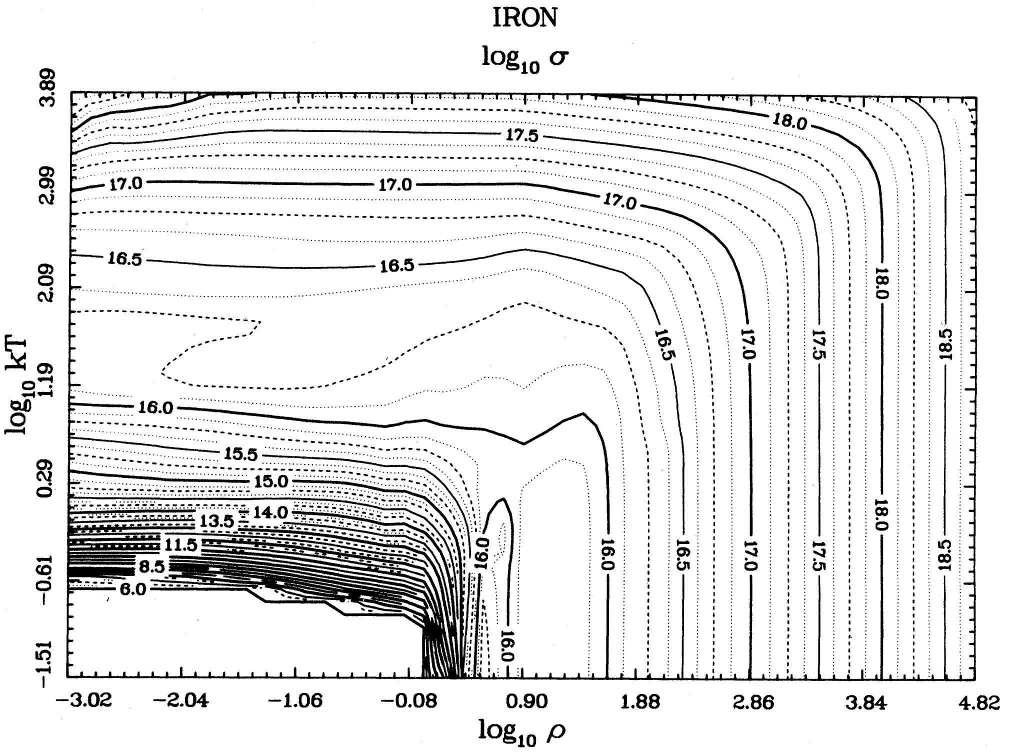

FIG. 2. Electrical conductivity σ (s^{-1}) as a function of temperature and density.

TABLE I. Comparison of calculated electrical resistivity η_c ($\mu\Omega$ cm) and experimental resistivity η_x for solid and liquid iron.

Phase	ρ (g/cm^3)	T (K)	η_c	η_x	$\frac{1}{\eta_c}\frac{d\eta_c}{dT}$	$\frac{1}{\eta_x}\frac{d\eta_x}{dT}$
Solid	7.86	293	135	9.7[a]	1.3×10^{-5}	6.5×10^{-3}
Solid	7.36	1810	126	127.5[b]	1.1×10^{-5}	
Liquid	7.05	1810	118	138.6[b]	1.0×10^{-5}	2.4×10^{-4}

[a] Reference 14.
[b] Reference 15.

Lampe's explicit expressions for S_{ij} are rather lengthy and will not be reproduced here. In addition to the Coulomb logarithms, they involve generalized Fermi-Dirac integrals, which account for the electron statistics. Accurate expressions for these integrals have not been available previously. For the present application, Fullerton[8] has obtained highly efficient 10-decimal Chebyshev approximations. These approximations are effective except in cases of extreme electron degeneracy ($\mu/kT > 10^4$, where μ is the chemical potential). The approximations fail because Lampe's expressions contain combinations of the functions that ultimately become numerically unstable. These combinations include terms with as many as five factors of the integrals to be evaluated. Each integral has an asymptotic expansion of the form

$$I_j(z) \rightarrow z^j \sum_{i=0}^{\infty} a_i z^{-i} \quad \text{as } z \rightarrow \infty , \tag{4}$$

where $z=\mu/kT$ is the degeneracy parameter. The instabilities arise through cancellation of the leading terms in z. In principle, the expansions and series manipulations can be done analytically to extract the surviving terms. Instead, we have chosen the easier and equivalent method of simply evaluating Fullerton's approximations, combining them, and determining the asymptotic coefficients numerically before instability sets in.

As an example of the application of this procedure, we consider the computation of the remaining transport coefficients from our previous results for the ionization state and electrical conductivity of iron at various temperatures and densities.[3] Figures 1—6 show numerically computed function values for temperatures and densities on a logarithmic grid. Temperatures range from 10^{-2} to 10^4 eV, and densities range from 3×10^{-4} to 10^5 g/cm^3. Figure 1 (see Fig. 12 of I) shows the ionization state Z_i as a contour plot. At very low densities, the ionization state ap-

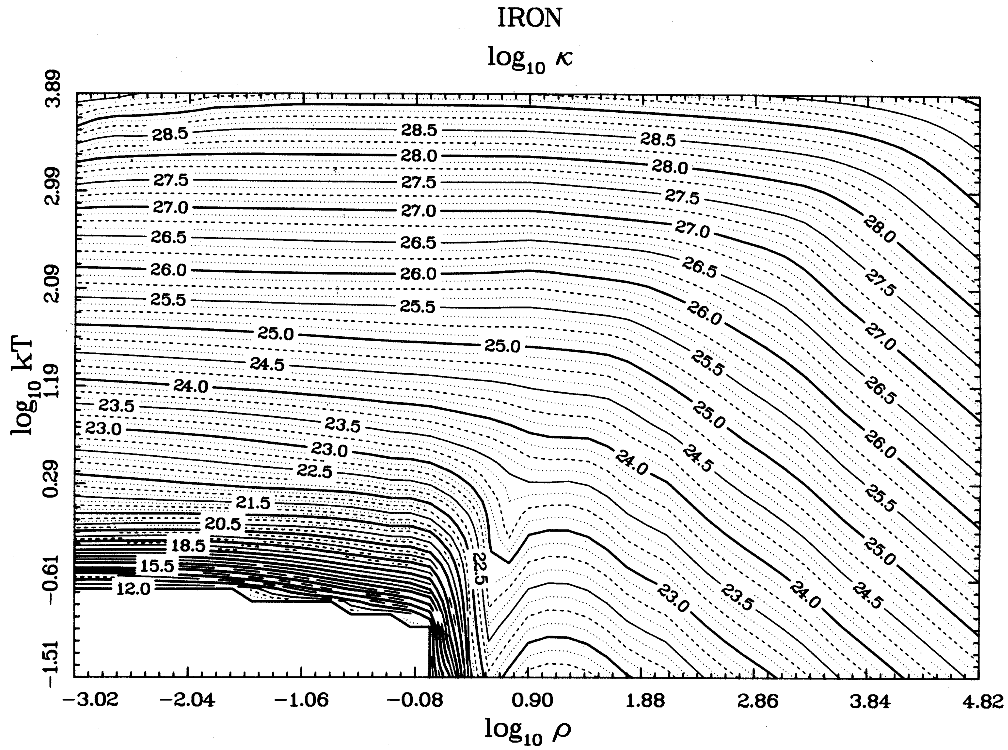

FIG. 3. Thermal conductivity κ (cm^{-1} s^{-1}) as a function of temperature and density.

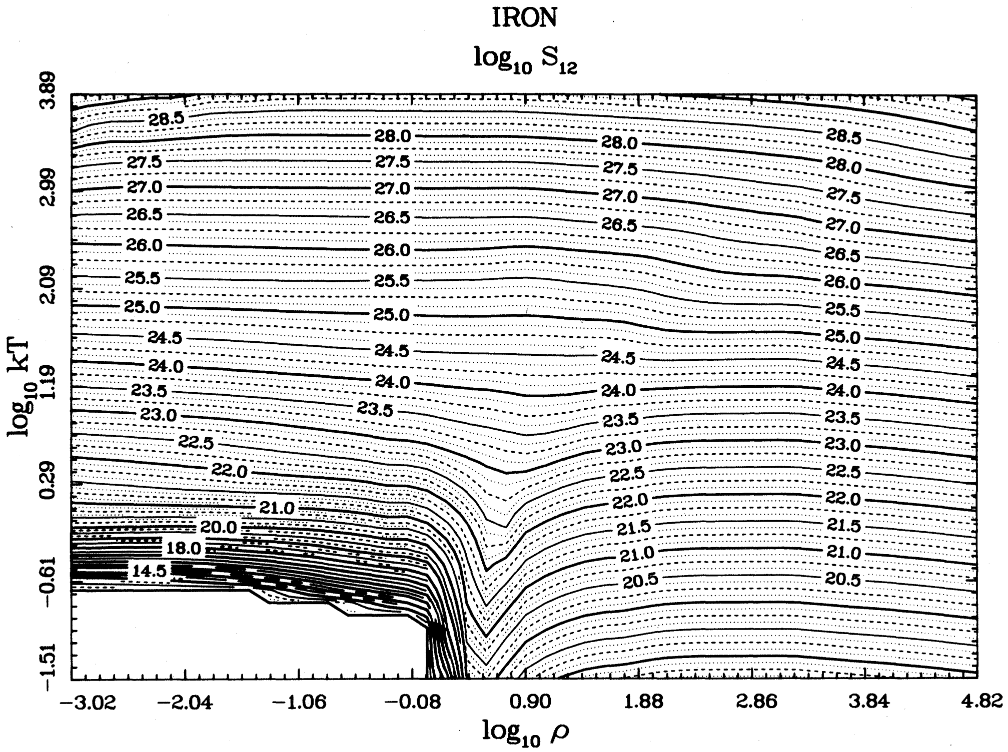

FIG. 4. Thermoelectric coefficient S_{12} ($\mathrm{cm}^{-1}\,\mathrm{s}^{-1}$) as a function of temperature and density.

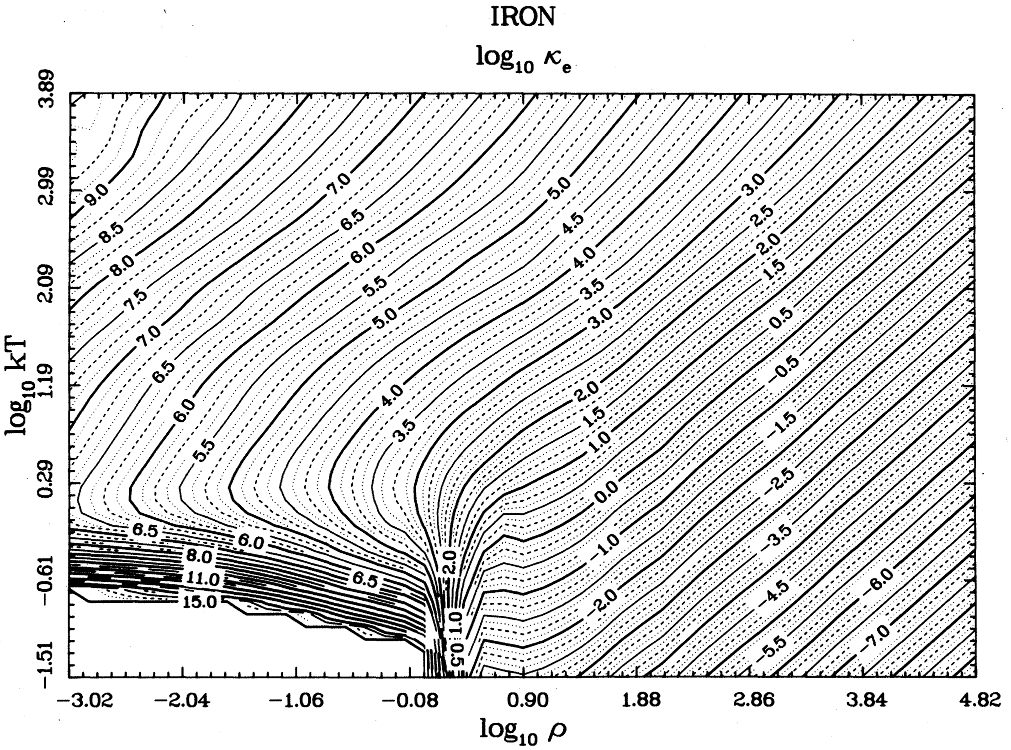

FIG. 5. Electron conductive opacity κ_e ($\mathrm{cm}^2\,\mathrm{g}^{-1}$) as a function of temperature and density.

TABLE II. Comparison of calculated thermal conductivity κ_c ($\mathrm{erg\,K^{-1}\,s^{-1}\,cm^{-1}}$) and experimental conductivity κ_x for solid iron at zero pressure.

ρ (g/cm^3)	T (K)	κ_c	κ_x[a]
7.86	300	0.55×10^6	8.03×10^6
7.76	600	1.10×10^6	5.47×10^6
7.66	900	1.68×10^6	3.80×10^6
7.56	1200	2.26×10^6	2.82×10^6
7.46	1500	2.86×10^6	3.18×10^6

[a] Reference 16.

proaches zero as $kT\rightarrow0$ because sufficient bound states are formed to accommodate all electrons. The onset of thermal ionization as kT increases and of pressure ionization as ρ increases is readily apparent. Surface irregularities arise from shell structure in the partial-wave analysis. The transport coefficients are strongly coupled to these ionization states in the present model.

Figure 2 (see Fig. 13 of I) shows the electrical conductivity σ in the units $\mathrm{s^{-1}}$. The sharp peak near normal density at small kT arises from the ionization of the $4s$ and $3d$ states and the strong d-wave scattering, which makes iron a transition metal. In other regions of ρ and kT, the behavior of its electrical conductivity is more nearly normal.

Virtually no experimental conductivity data exist in the regions of temperature and density for which our model is strictly applicable. The only clear point of comparison is the electrical resistivity of the liquid at melting point, as discussed in I. Here, our model gives the surprisingly good result of 118 $\mu\Omega\,\mathrm{cm}$, compared with the experimental value of 138.6. Table I gives additional comparisons for the solid phase at room temperature and at the melting point. The inapplicability of the model for the solid phase is readily apparent. The calculated temperature dependence is negligible, whereas experimentally, the resistivity decreases dramatically as the temperature is decreased. This presumably arises from additional transport processes not considered here.

Figure 3 shows the thermal conductivity κ in units $\mathrm{cm^{-1}\,s^{-1}}$. The transition-metal peak in the electrical conductivity (see Fig. 2 of this paper, and Fig. 13 of I) is smaller in relative magnitude because of the additional process of electron-electron scattering, which does not contribute to the electrical conductivity. Table II gives comparisons with experimental measurements for the solid phase. As with the electrical conductivity, the agreement is good near the melting point but deteriorates as the temperature is lowered. The experimental values decrease with temperature at first but then rise as additional transport processes become active, whereas the calculated values decrease monotonically. Experimental measurements are not available for the liquid phase.

Figure 4 shows the thermoelectric coefficient S_{12} in $\mathrm{cm^{-1}\,s^{-1}}$. Figure 5 shows the conductive opacity κ_e in $\mathrm{cm^2\,g^{-1}}$. This quantity is related simply to the thermal conductivity by

$$\kappa_e=\frac{16}{3}\frac{\sigma_{sb}}{k}\frac{T^3}{\rho\kappa}\,, \tag{5}$$

where

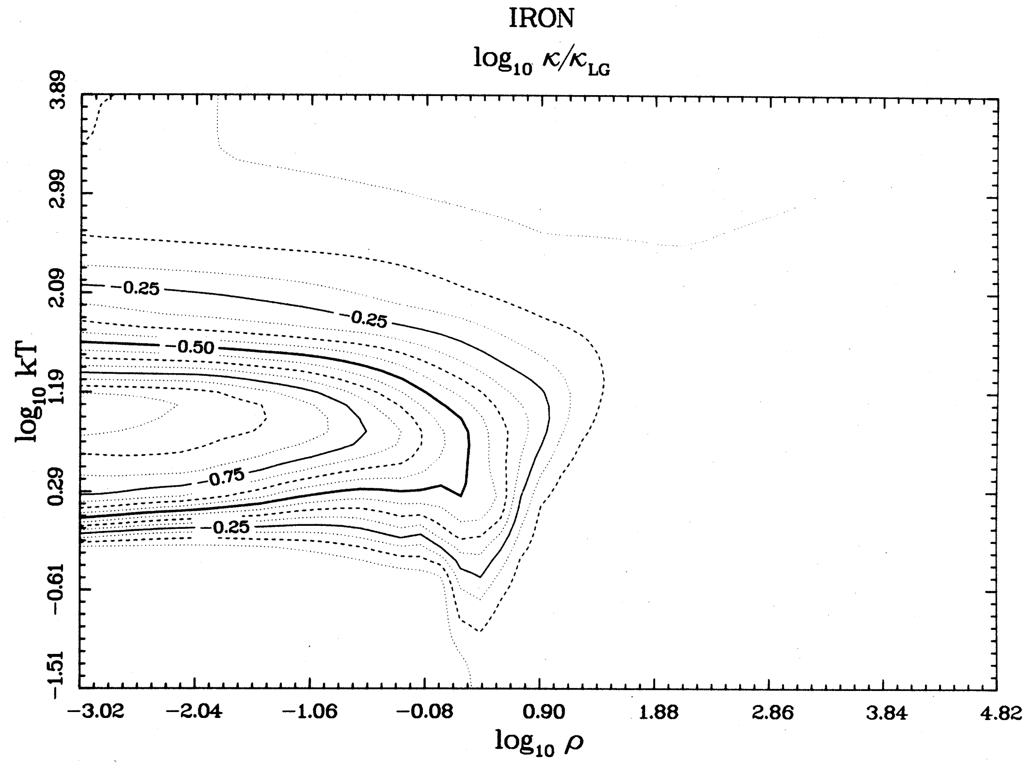

FIG. 6. Ratio of calculated thermal conductivity κ to the Lorentz gas (LG) value κ_{LG}.

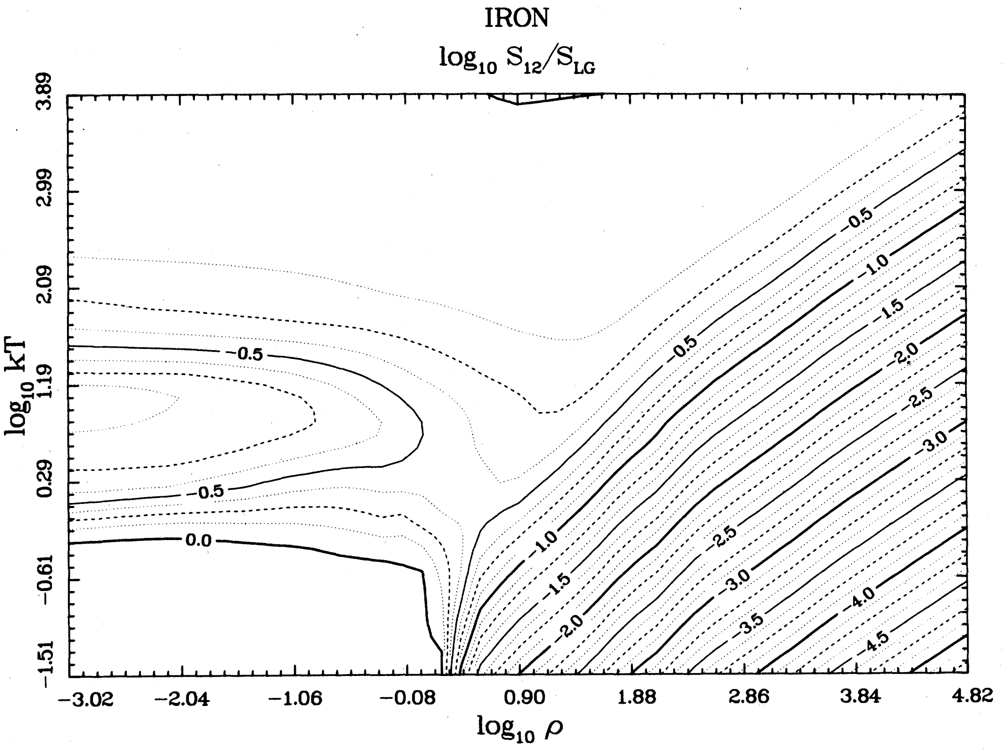

FIG. 7. Ratio of calculated thermoelectric coefficient S_{12} to the Lorentz gas value S_{LG}.

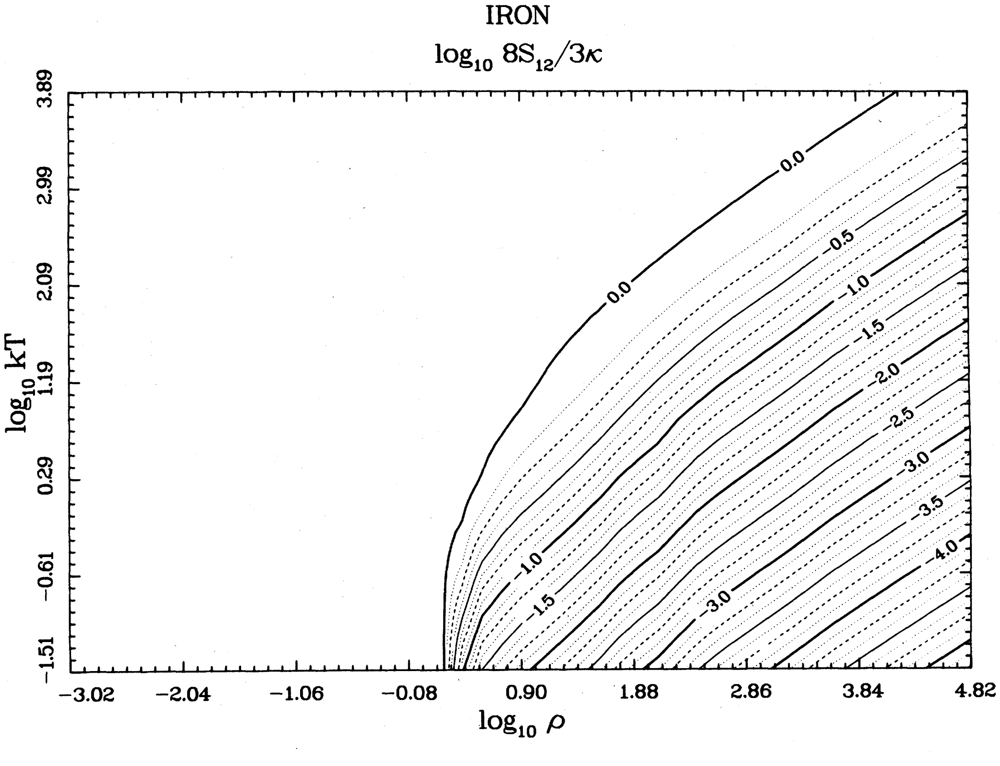

FIG. 8. Deviations from the Lorentz gas model in the ratio of thermoelectric coefficient S_{12} to thermal conductivity κ.

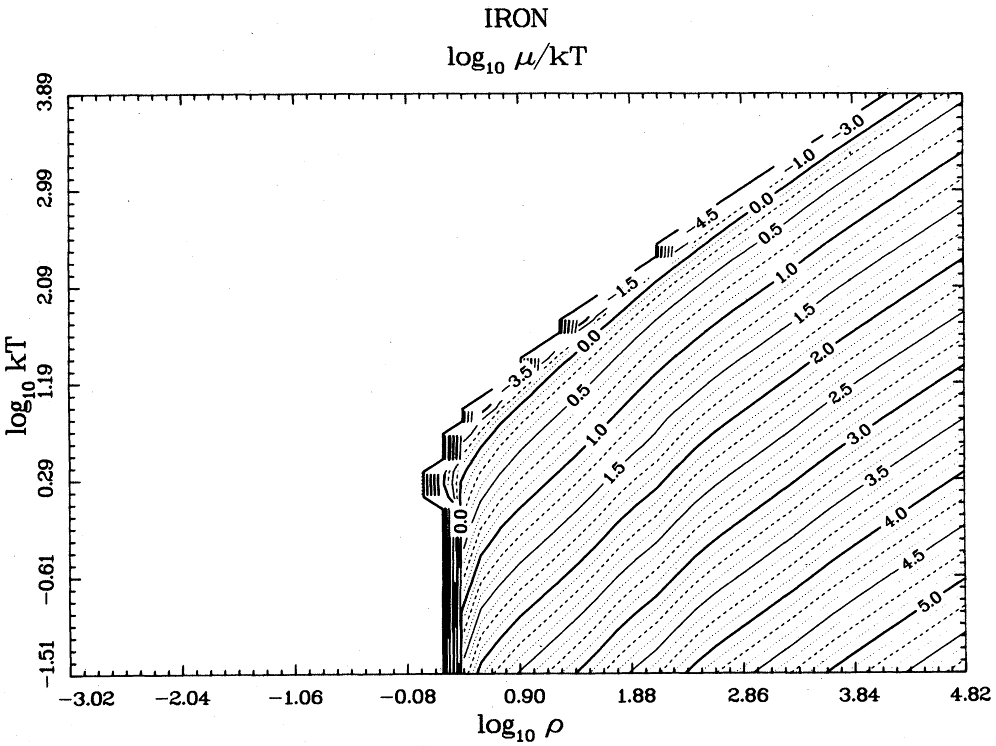

FIG. 9. Degeneracy parameter μ/kT as a function of temperature and density.

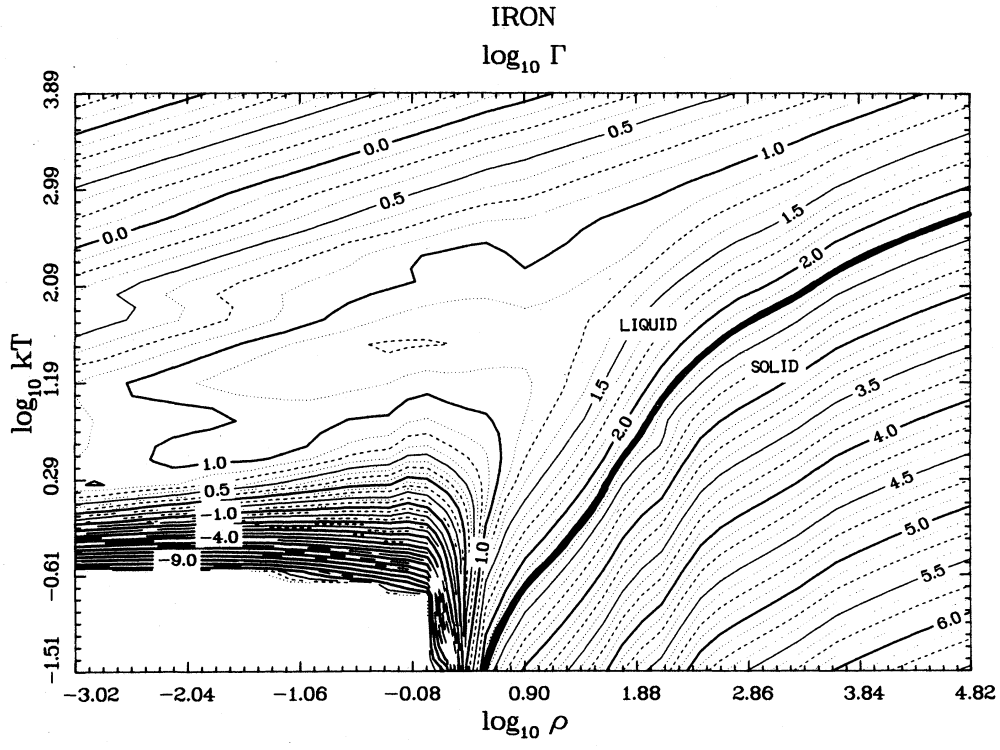

FIG. 10. Ion-ion coupling constant Γ as a function of temperature and density.

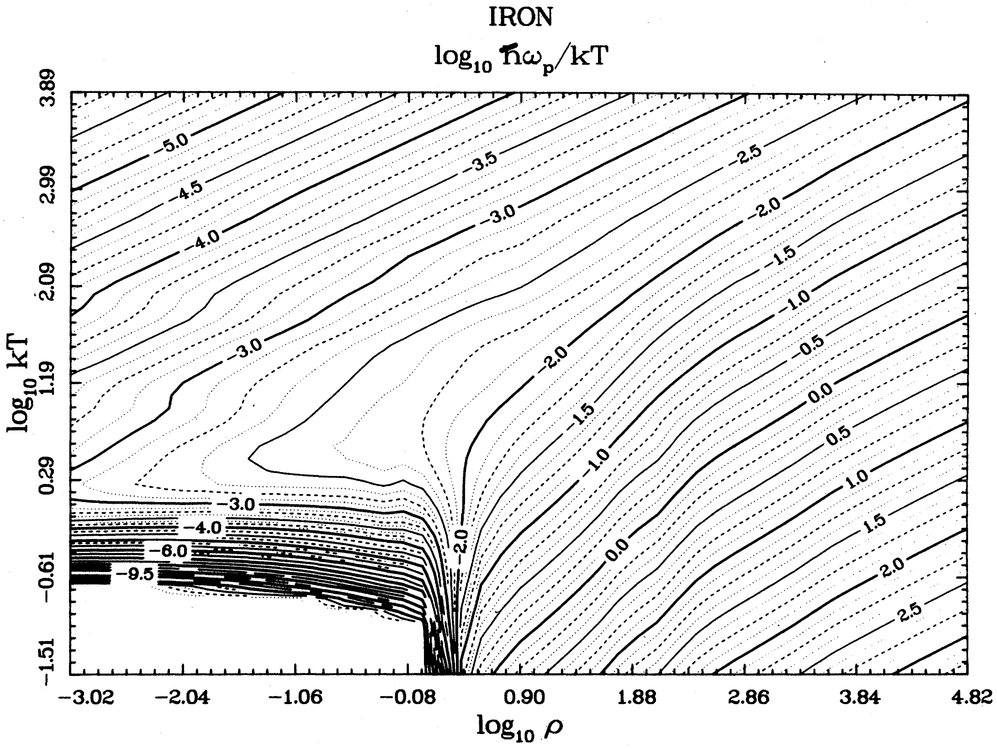

FIG. 11. Plasma frequency $\hbar\omega_p/kT$ as a function of temperature and density.

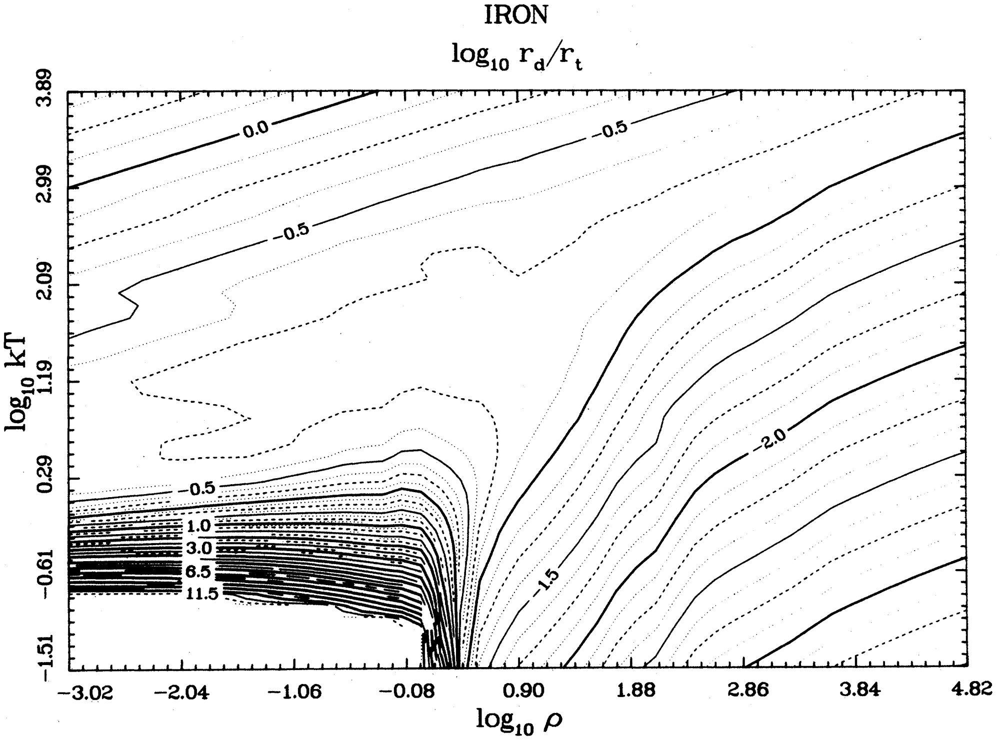

FIG. 12. Ionic Debye radius r_d/r_t as a function of temperature and density.

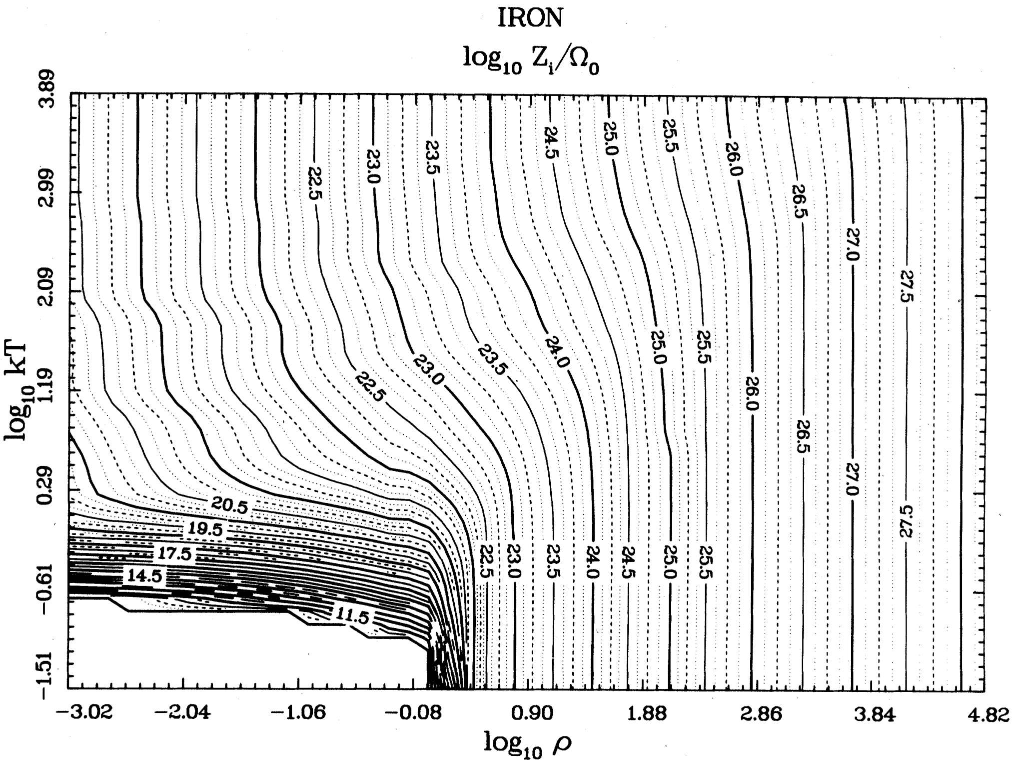

FIG. 13. Free-electron number density $n_e = Z_i/\Omega_0$, where Ω_0 is the ionic volume in cm^3.

$$\sigma_{sb}/k = 4.10696\times 10^{11}\,\mathrm{s}^{-1}\,\mathrm{cm}^{-2}\,\mathrm{K}^{-3} . \tag{6}$$

It is included here for convenient comparison with radiative opacities.

Figures 6–8 give comparisons with the (degenerate) Lorentz gas model, which neglects electron-electron contributions to thermal conduction and yields the simple relationships

$$\kappa = \frac{4kT}{\alpha\hbar c}\sigma \tag{7}$$

and

$$S_{12} = \tfrac{3}{8}\kappa . \tag{8}$$

Figure 6 shows the ratio of the thermal conductivity to the Lorentz gas result. Deviation from 1 in this ratio indicates the importance of electron-electron collisions. (Nondegeneracy corrections to the Lorentz gas affect this ratio by less than 10% throughout this figure.) Electron-electron collisions are important at intermediate temperature and low density. Throughout the remainder of the range calculated, the discrepancy is less than 25%. Figure 7 shows the same for the thermoelectric coefficient. In addition to the above region of importance, very large deviations occur in regions of high degeneracy (low temperature and high density). This arises[1] from subtraction of the convective heat flux from S_{12} in Eq. (1) but not in Eq. (8). Figure 8 shows the ratio $8S_{12}/3\kappa$, which is identically 1 in the degenerate Lorentz gas model. This ratio remains close to 1 in the present calculation even in the region where electron-electron collisions are important, but as with the thermoelectric coefficient itself, large deviations occur for high degeneracy.

Figure 9 displays the degeneracy parameter μ/kT. The dramatic change from a nondegenerate system to a degenerate system at high density and low temperature is readily apparent.

The ion-ion coupling constant

$$\Gamma = \frac{Z_i^2 \alpha\hbar c}{kTr_t} \tag{9}$$

is plotted in Fig. 10. One-component plasma calculations indicate crystallization at $\Gamma \simeq 170$ for any material. A rough semiempirical check on this value is given by evaluating our model at the zero-pressure melting temperature. Values at the experimental solid and liquid densities are $\Gamma = 204$ and 190, respectively. On the scale of the figures, differences between these values of Γ are hardly visible. The heavy line in Fig. 10 at $\log_{10}\Gamma \simeq 2.25$ indicates this phase transition.

Figure 11 shows the plasma frequency

$$\left[\frac{\hbar\omega_p}{kT}\right]^2 = \frac{3(\hbar c)^2}{kTr_t^2 M_N c^2}\Gamma , \tag{10}$$

where M_N is the nuclear mass. Figure 12 shows the ionic Debye radius

$$\frac{r_d}{r_t} = (3\Gamma)^{-1/2} , \tag{11}$$

where r_t is the Wigner-Seitz radius (see I). This parameter becomes too small to be meaningful well inside the solid-phase region. Figure 13 displays the free-electron number density per unit volume in Å^{-3}.

We expect the present results to be reliable throughout the region $\Gamma < 200$ (see Fig. 10). They should be particularly useful because they extend the region of feasible calculation well beyond the limits imposed by Born approximation (compare Figs. 10 and 15 of I; see also Refs. 9 and 10).

Difficulties are encountered near the metal-insulator phase transition at low temperature. These difficulties arise from the sensitivity of our results to ionic shell structure. This shell structure can be adjusted within limits by altering the potentials used, but great significance cannot be attached to the results. In reality, the problem in this region of temperature and density involves the interaction of a great many degrees of freedom in the absence of long-range order and is so far not amenable to accurate solution.

Further difficulties arise for $\Gamma > 200$. In this region, crystallization occurs, and it is clear (see Tables I and II) that our approach quickly becomes inadequate as the crystal becomes more tightly bound in relation to the temperature. Some efforts have been made to account for these effects in a systematic way.[11–13] We have investigated purely empirical adjustment schemes to force our results to fit solid-state experimental data. It is not particularly difficult to produce accurate fits, but whether extrapolation of these fits into experimentally unavailable regions can be expected to make sense remains to be seen.

ACKNOWLEDGMENT

I would like to thank L. W. Fullerton for responding to a request for routines to calculate the generalized Fermi-Dirac integrals.

---

[1] M. Lampe, Phys. Rev. **170**, 306 (1968); **174**, 276 (1968).

[2] R. Balescu, *Statistical Mechanics of Charged Particles* (Interscience, New York, 1963).

[3] G. A. Rinker, preceding paper [Phys. Rev. B **31**, 4207 (1985)].

[4] G. A. Rinker, Los Alamos National Laboratory Report LA-9872-MS, January, 1984 (unpublished).

[5] G. A. Rinker, Los Alamos National Laboratory Report LA-10202-MS, November, 1984 (unpublished).

[6] See AIP document No. PAPS PRBMD-31-4207-33 for 33 pages of technical appendices. Order by PAPS number and journal reference from American Institute of Physics, Physics Auxiliary Publication Service, 335 East 45th Street, New York, N.Y. 10017. The price is $1.50 for a microfiche, or $5.00 for a photocopy. Air mail additional. Make checks payable to the American Institute of Physics.

[7] D. B. Boercker, F. J. Rogers, and H. E. DeWitt, Phys. Rev. A **25**, 1623 (1982).

[8] L. W. Fullerton, *Numerical Techniques for Generalized Fermi-Dirac Integrals* (Coyote, Velarde, 1982).

[9] N. Itoh, S. Mitake, H. Iyetomi, and S. Ichimaru, Astrophys. J. **273**, 774 (1983).

[10] S. Mitake, S. Ichimaru, and N. Itoh, Astrophys. J. **277**, 375 (1984).

[11] W. B. Hubbard and M. Lampe, Astrophys. J. Suppl. Ser. **18**, 297 (1969).

[12] Y. T. Lee and R. M. More, Phys. Fluids **27**, 1273 (1983).

[13] N. Itoh, Y. Kohyama, N. Matsumoto, and M. Seki, Astrophys. J. (to be published).

[14] *CRC Handbook of Chemistry and Physics*, edited by R. C. Weast (Chemical Rubber, Boca Raton, 1983), p. F-125.

[15] J. R. Wilson, Metall. Rev. **10**, 381 (1965).

[16] *CRC Handbook of Chemistry and Physics*, edited by R. C. Weast (Chemical Rubber, Boca Raton, 1983), p. E-9.